ANALYTICAL SEISMIC PERFORMANCE ASSESSMENT OF BRACED TIMBER FRAMES WITH SHAPE MEMORY ALLOY FASTENERS

Javier Fierro[1], Daniel Lacroix[2], Eugene Kim[3]

ABSTRACT: Braced timber frames (BTFs) are an efficient structural system to resist earthquake forces; however, their performance significantly relies on the behaviour of the brace connection, which absorbs seismic energy through fastener yielding and wood crushing, resulting in strength and stiffness degradation with residual deformations. Recent research indicates dowel-type wood-steel connections with superelastic NiTi (nickel titanium) shape memory alloy (SMA) fasteners exhibit substantial self-centering behaviour under cyclic loading compared to conventional steel fasteners. This study analytically evaluates the self-centering capability of a single-story BTF using SMA dowel-type fasteners and compares their seismic performance to traditional steel fasteners using numerical models in OpenSees. Experimental results were used to calibrate the connection-level hysteretic behaviour. The seismic analysis of wood-frame structures (SAWS) and the dowel-type exponential (DTE) models available in OpenSees were utilized to simulate the connection behaviour within BTFs. Overall, the analysis demonstrates that BTFs with SMA fasteners can exhibit significant self-centering ability and reduced residual deformation compared to BTFs using conventional steel dowels. Additionally, the effect of SMA connections on seismic response and residual drift under representative ground motions for moderate seismicity in Eastern Canada is discussed.

KEYWORDS: braced timber frames, seismic performance, shape memory alloy, self-centering, frame-level model

1 – INTRODUCTION

Braced timber frames (BTFs) are a sustainable and effective lateral force-resisting systems for buildings subject to earthquakes or winds loads [1]. Due to their lightweight nature and ductile connections, BTFs exhibit desirable seismic performance, making them suitable for regions with moderate seismic activity, such as Eastern Canada, where there is a growing demand for resilient timber structures [2]. However, the Canadian design standard, *Engineering design in wood,* [3] provides limited information on adequate connection detailing to achieve acceptable ductility and seismic performance.

Experimental studies have developed the foundational knowledge of the seismic behaviour of BTFs [4–7]. Recent research on BTFs has focused on relating the connection ductility to the system ductility to inform design guidelines in the CSA O86 standard [2, 8]. Chen and Popovski [8] showed that the required connection ductility decreases significantly if both ends of the brace yield simultaneously; however, this is not the case in most scenarios even if the dowels yield in a ductile manner. Baird et al [9] experimentally confirmed bolt yielding and wood crushing as critical factors controlling the brace behaviour, achieving ductility ratios of 7.1 to 8.1 under semi-cyclic loading. Furthermore, novel systems like timber buckling-restrained braces (BRBs) have shown a great deal of promise for improving the seismic resilience of BTFs by offering high energy dissipation and ductility [10–12].

In addition, numerical studies on BTFs have allowed for a more complete analysis of seismic behavior using parametric analyses and system-level simulations. These models have helped advance design by capturing critical cyclic response features such as pinching, stiffness deterioration, and strength loss. One of the most extensively used hysteretic models for timber structures is the seismic analysis of woodframe structures (SAWS) model [13]. Similarly, the dowel-type exponential (DTE) model by Dong et al [14] can accurately simulate

[1] Javier Fierro, Research Assistant, Department of Civil & Environmental Engineering, University of Waterloo, 200 University Ave West, Waterloo, N2L 3G1, Ontario, Canada, jsfierro@uwaterloo.ca

[2] Daniel Lacroix, Assistant Professor, Department of Civil & Environmental Engineering, University of Waterloo, 200 University Ave West, Waterloo, N2L 3G1, Ontario, Canada, daniel.lacroix@uwaterloo.ca, ORCID: https://orcid.org/0000-0003-2002-3827

[3] Eugene Kim, Assistant Professor, Department of Civil & Environmental Engineering, University of Waterloo, 200 University Ave West, Waterloo, N2L 3G1, Ontario, Canada, kekim@uwaterloo.ca, ORCID: https://orcid.org/0000-0001-8909-7918

https://doi.org/10.52202/080513-0183

the behavior of dowel-type timber joints. The work by Dong et al. [14] compared numerical simulations of the SAWS and DTE hysteretic models in OpenSees to experimental cyclic tests of dowel-type timber joints. The SAWS model gave fair approximations but continually overestimated stiffness at larger displacements, whereas the DTE model was more accurate, closely matching experimental data throughout the cyclic loading protocol.

In addition, the integration of innovative materials like shape memory alloys (SMAs) has recently emerged as a viable means to improve the seismic performance of timber connections. Because of their capacity to self-center, SMA dowels and tubes considerably reduce residual drift following seismic events [15, 16]. Recent studies [17, 18] have demonstrated how nickel-titanium or Nitinol (NiTi) SMA can be employed to increase the resiliency of timber structures under earthquake hazards by preserving connection integrity under significant cyclic displacements.

The current study analytically investigates the self-centering and seismic performance of single-story BTF using SMA dowel-type fasteners instead of conventional steel fasteners. In particular, the potential for reducing residual drift is assessed for a moderate seismic environment such as Eastern Canada. Calibrated hysteretic models based on experimental results are developed at the connection, brace, and frame levels using OpenSees [19]. The seismic response of traditional steel-dowel BTFs is compared to that of SMA-dowel BTFs in terms of self-centering behaviour and overall seismic performance.

2 – BACKGROUND

2.1 REFERENCE EXPERIMENT

Overview

Cléroux et al [18] investigated NiTi SMA dowels in dowel-type bolted connections with slotted-in steel plates in glulam braces for BTF systems, as an alternative to traditional steel dowels. The study evaluated connection-level performance through 24 tests -12 single-dowel and 12 four-dowel specimens- under monotonic and cyclic uniaxial loading. The four-dowel configuration was intended to simulate the behaviour of the reduced-scale BTF system connections. The study showed that SMA connections exhibited superior self-centering and minimal residual deformation, compared to steel counterparts under cyclic loads [18].

Experimental program

Figures 1a and 1b show the setup for testing four-dowel connections using a hydraulic frame. The glulam brace (127 × 140 × 500 mm^3, 20f-EX) was fixed to the frame bed via an overdesigned steel angle and A307 bolt connections to isolate deformations to the test connection. A 44W steel plate at the top was gripped by the actuator. The load was measured by the actuator's internal load cell, and displacements were recorded using two sensors mounted on the glulam and referenced from aluminum angles fixed to the steel plate. Displacement was averaged from both sensors.

Figure 1c displays the reduced-scale glulam-steel-glulam connection with an internal 6.35 mm 44W steel plate and four 6.35 mm dowels (steel or SMA), representative of multi-storey BTF applications. The glulam members were slotted, with a 20 mm end gap to avoid plate bearing in compression. The fastener layout followed CSA O86 [3], targeting ductile failure modes (ref. to Cléroux et al [18]).

The tests followed ASTM E2126 [20], where failure was defined as a 20% drop in maximum capacity or the onset of secondary failures under monotonic loading (ref. to Cléroux et al [18]). For the cycle tests, the Method B procedure with a maximum displacement of 12 mm was followed. This resulted in full reversed cyclic loading restricted to a displacement of 12 mm, even though higher displacements were observed under monotonic loading because both steel and SMA fasteners exhibited brittle cyclic shear failure and permanent deformation after this targeted displacement [18].

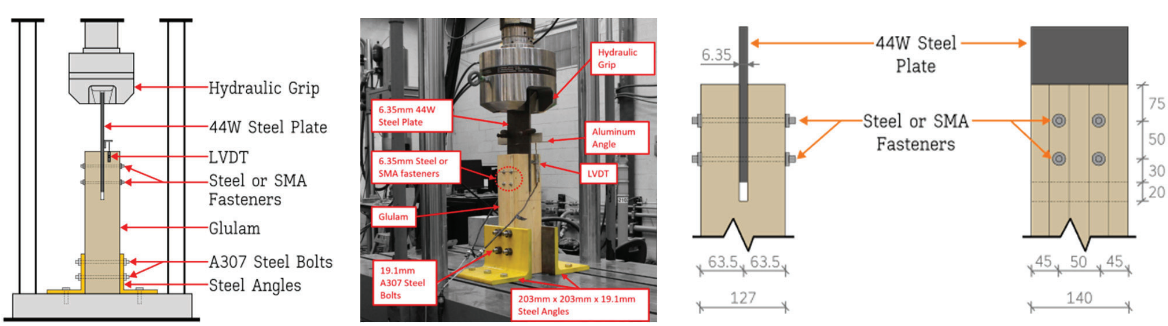

a) schematic test setup *b) test setup* [18] *c) connection details. Adapted from* [18]

***Figure 1:** Experimental four-bolt connection setup*

https://doi.org/10.52202/080513-0183

Monotonic testing on steel and SMA connections revealed substantial deformation in bolts, resulting in wood parallel-to-grain row shear failure. The steel connection tested to ultimate failure experienced an abrupt resistance drop at around 33 mm displacement, coincident with wood shear failure while a similar failure was observed with the SMA connection at a lesser displacement of approximately 17 mm [18]. Cléroux et al [18] further evaluated the results of these monotonic curves at a displacement of 14 mm in order to directly contrast them with cycle tests. At this displacement, SMA connections were able to resist approximately 23% more loads than steel connections, although having a 12% lower initial stiffness [18].

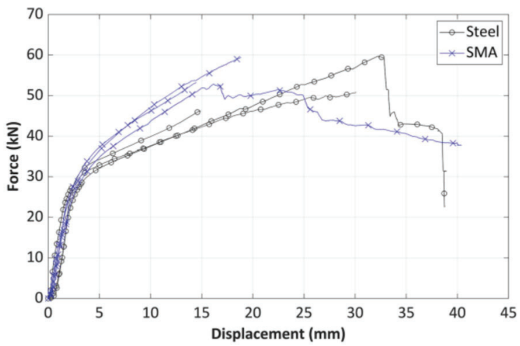

Figure 2: *Monotonic four-bolt connection curve* [18]

For the cyclic force-displacement curves, both steel and SMA connections demonstrated stable hysteresis. Steel connections plateaued in strength and exhibited wide loops with offset unloading paths, indicating residual deformation. SMA connections showed loading and unloading branches passing through the origin, indicating self-centering behaviour. This was observed in the absence of permanent distortion in the SMA bolts due to their superelastic behavior during unloading [18].

While the SMA bolt connections showed superior strength and comparable deformation ability to their steel counterparts, the failure was sudden unlike the gradual softening observed in the steel bolts failure [18]. Both failure modes could be characterized as Mode "g" per CSA O86 [3] or Mode *IV* of the European Yield Model [21]. Table 1 summarizes the cyclic test results where the SMA connections showed at least 20% higher yield strength and up to 30% greater peak and ultimate loads in compression. Both connections exhibited reduced strength in cyclic tests due to earlier dowel failure at lower displacements [18].

3 – NUMERICAL MODELLING

3.1 CONNECTION-LEVEL MODEL

Numerical models were developed to replicate the connection behaviour observed in Cléroux et al [18]. Plastic hinge models using OpenSees zeroLength elements were implemented to simulate the nonlinear response based on experimental data. The model is shown in Figure 3 and consists of a zeroLength element (11) connecting two nodes: Node (1) is fixed, while Node (2) is restrained against horizontal translation and out-of-plane rotation. The x-direction response, defined by the assigned uniaxial material, captures the connection's behaviour.

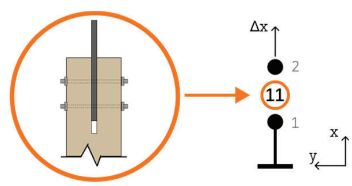

Figure 3: *Plastic hinge (zeroLength element) model*

Experimental results from six four-bolt cyclic tests -three steel (4SC.1–3) and three SMA (4NC.1–3)- were used for model calibration. Connection behaviour was modelled

Table 1: *Connection Properties of Cyclic Connections. Adapted from* **[18]**

Specimen	P_y [a] (kN)	Δ_{Py} [b] (mm)	P_{peak} [c] (kN)	Δ_{Ppeak} [d] (mm)	P_u [e] (kN)	Δ_{Pu} [f] (mm)	K [g] (N/mm)	μ [h]
Steel								
1	19.7	1.6	31.1	7.8	24.9	11.1	13.5	7.0
2	13.3	1.0	29.8	5.7	23.9	10.6	13.0	10.4
3	13.5	1.1	30.9	5.7	24.7	10.6	11.7	9.4
Avg.	15.5	1.2	30.6	6.4	24.5	10.8	12.7	8.9
CoV	0.19	0.20	0.02	0.16	0.02	0.02	0.06	0.16
SMA								
1	23.6	1.8	39.9	7.7	31.9	11.0	13.8	6.2
2	25.3	2.4	41.8	8.6	33.4	11.2	12.5	4.6
3	23.2	2.8	42.7	10.6	34.1	12.1	9.0	4.2
Avg.	24.1	2.4	41.5	8.9	33.2	11.4	11.8	5.0
CoV	0.04	0.19	0.03	0.13	0.03	0.04	0.17	0.17

[a] *Yield load determined using the Y & K method*
[b] *Yield displacement*
[c] *Peak load*
[d] *Displacement at peak load*
[e] *Ultimate load*
[f] *Displacement at ultimate load*
[g] *Stiffness of connection (slope from 10% to 40% of P_y)*
[h] *Ductility defined as Δ_{Pu} divided by Δ_{Py}*

https://doi.org/10.52202/080513-0183

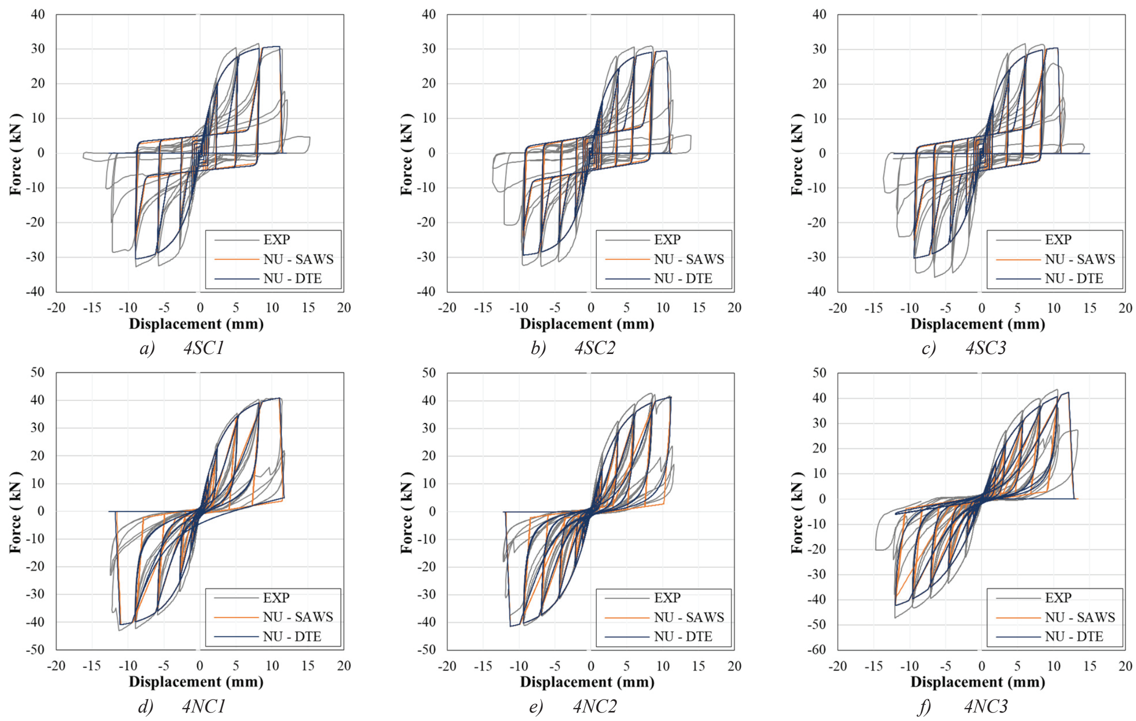

a) 4SC1 *b) 4SC2* *c) 4SC3*

d) 4NC1 *e) 4NC2* *f) 4NC3*

***Figure 4:** Experimental four-bolt connection setup*

using two OpenSees uniaxial materials, SAWS [13] and DTE [14]. The calibration was based on parameters from Table 1 and the experimental hysteresis curves. Figure 4 compares the experimental and numerical results.

Numerical models showed good agreement with test data, capturing the post-yield cyclic behaviour of both steel and SMA connections. Steel models exhibited gradual strength gain and stable loops, while SMA models showed increased strength until failure, matching the experimental response. The models effectively reproduced key behaviour: stiffness degradation and permanent deformation in steel unloading branches, and the distinct loading and unloading responses in the SMA. Although both material models adequately captured the load-deformation behaviour, the DTE model yielded better captured slope transitions at displacement intercepts. The curves display that steel loops showed greater energy dissipation, while SMA loops were narrower.

The parameters of the DTE and SAWS models, calibrated individually against experimental results (Figure 4), were averaged to obtain representative hysteretic response curves, as shown in Figure 5. These averaged responses form the basis for evaluating system-level performance and comparing SMA against conventional steel connections in further pushover and time history analyses.

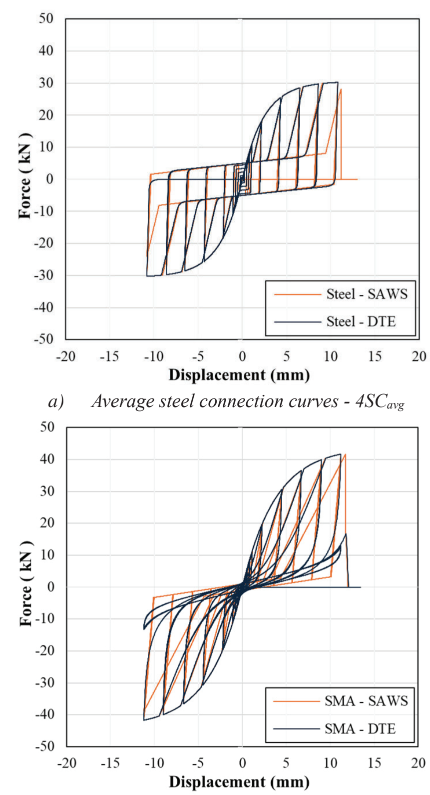

a) Average steel connection curves - $4SC_{avg}$

b) Average SMA connection curves – $4NC_{avg}$

***Figure 5:** Plastic hinge connections*

https://doi.org/10.52202/080513-0183

3.2 BRACE-LEVEL MODEL

Strong and weak connections

The initial brace-level models used a linear elastic element (111) to represent the timber brace and two identical nonlinear springs (11) to model the connections, assuming symmetric behaviour (Figure 6a). However, literature [4, 6, 7, 9, 22] shows that brace connections often deform unevenly. Cyclic tests by Popovski [4] showed that material and fabrication variability caused one end of the brace to deform more, concentrating most of the nonlinear deformation at one connection. As a result, one connection typically experiences greater initial deformation and wood crushing, entering nonlinear behaviour earlier. As its stiffness reduces, it attracts more deformation, leading to failure. This one is described as the weak connection while the other is the strong connection [7]. Given the natural variability of wood as a structural material, it is difficult to predict which connection will be weak or strong. However, the locations of the weak and strong connections do not affect the overall brace-level and can be used interchangeably in the model.

Chen and Popovski [8] state that using a conventional modelling approach with two identical connections results in an overestimation of brace energy dissipation and ductility. They proposed a brace model with a timber element (stiffness K_b) and two connection springs (stiffness K_c) in series as shown in Figure 6b. The authors also note that the weak connection has a lower yield strength compared to the strong connection and absorbs nearly all the nonlinear deformations, resulting in the brace assembly's yield strength, F_{bay}, being governed by the weaker connection, F_{cwy} [8]. The yield displacement of the brace assembly is then calculated as the sum of the deformation contributions from the weak connection, the brace, and the strong connection, based on the yield force of the weak connection, F_{cwy}, such as:

$$\Delta_{bay} = 2\frac{F_{cwy}}{K_c} + \frac{F_{cwy}}{K_b} \qquad (1).$$

Since the stiffness of both connections is equal, $K_{cw} = K_{cs}$, the system stiffness in the elastic range ($K_{e,y}$) is:

$$K_{e,y} = \frac{1}{\frac{1}{K_{cw}} + \frac{1}{K_{cs}} + \frac{1}{K_b}} = \frac{1}{\frac{2}{K_{cw}} + \frac{1}{K_b}} \qquad (2).$$

For plastic behaviour, the ultimate brace displacement (Δ_{bau}) combines the weak connection's ultimate displacement (Δ_{cwu}), and the elastic yield displacements of the strong connection and timber brace:

$$\Delta_{bau} = \Delta_{cwu} + \frac{F_{cwy}}{K_c} + \frac{F_{cwy}}{K_b} \qquad (3).$$

Based on equation (3), the strong connection is assumed rigid once yielding occurs, contributing no additional deformation. As a result of this simplification, the system deformation is then primarily due to the weak connection, which is compatible with the equations presented by Chen and Popovski [8]. Therefore, the system-level plastic stiffness ($K_{e,p}$) is:

$$K_{e,p} = \frac{1}{\frac{1}{K_{cw}} + \frac{1}{K_b}} \qquad (4).$$

The final brace-level model includes the calibrated nonlinear weak connection (11), the elastic-response-based strong connection (12), and a linear timber brace (111), as shown in Figure 6c.

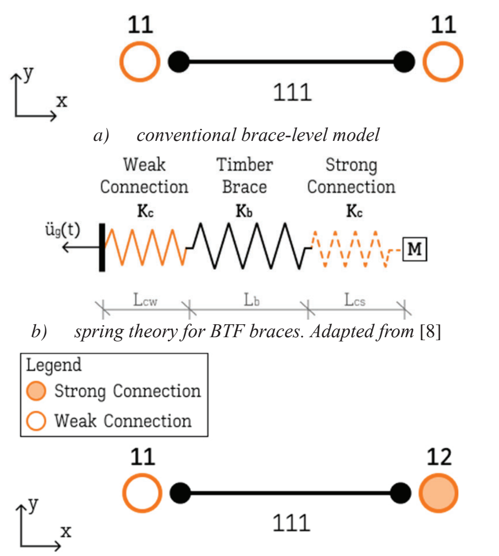

a) conventional brace-level model

b) spring theory for BTF braces. Adapted from [8]

c) strong and weak connections in brace-level model

Figure 6: *Brace-level models studied*

Numerical model validation

In this study, the brace-level models developed in OpenSees align with the equivalent nonlinear connector element proposed by Chen and Popovski [8] for simulating brace behaviour with weak and strong connections. This element was used in various multistorey building prototypes to estimate system ductility. Reported differences between numerical and predicted ductility values were within ±5% [8].

A numerical model based on the framework in Figure 6c was created to study brace behaviour under uniaxial loading parallel to the grain. One end of the brace was fixed and the other loaded in tension. Since brace response is independent of weak/strong connection positioning, the

https://doi.org/10.52202/080513-0183

Table 2: *Spring Theory and OpenSees Brace Model Results*

Model	**ST**		**OS - DTE**				**OS - SAWS**			
	$D_{ba,y}$	$D_{ba,u}$	$D_{ba,y}$		$D_{ba,u}$		$D_{ba,y}$		$D_{ba,u}$	
4SC1	3.36	13.00	3.66	9.0%	13.18	1.4%	3.67	9.3%	13.18	1.4%
4SC2	2.34	11.92	2.02	-13.7%	12.17	2.1%	2.02	-13.7%	12.13	1.8%
4SC3	2.61	12.05	2.15	-17.6%	12.20	1.2%	2.14	-17.9%	12.20	1.2%
$4SC_{avg}$	2.79	12.36	2.55	-8.5%	12.46	0.8%	2.54	-8.8%	12.42	0.4%
4NC1	3.94	13.23	3.98	0.9%	13.64	3.1%	4.05	2.7%	13.64	3.1%
4NC2	4.61	13.79	5.04	9.3%	14.44	4.7%	5.04	9.3%	14.40	4.5%
4NC3	5.67	15.19	5.51	-2.8%	15.66	3.1%	5.48	-3.4%	15.55	2.3%
$4NC_{avg}$	4.62	13.98	4.85	5.0%	14.58	4.3%	4.85	5.0%	14.62	4.6%

fixed end was chosen arbitrarily. The timber brace (20f-EX glulam, 127 × 140 × 4000 mm) replicated the reference test setup and was assigned a modulus of elasticity of 10,300 MPa as per the CSA 086 [3].

Model accuracy was assessed by comparing yield and ultimate displacements from spring theory (ST) and OpenSees (OS). ST values were calculated using the weak connection parameters from Table 1 and Equations (1) and (3). Timber stiffness was calculated as 45 kN/mm. Table 2 presents yield and ultimate displacements for both ST and OS (DTE and SAWS) methods, including the percentage differences.

Comparison results show strong overall agreement. Most differences remain under 5%, although some yield displacement discrepancies were noted for both material models. The ultimate displacements of the steel models matched the ST values within 2% while the yield displacements were observed to range 0.82 – 1.09 times than those obtained using the theoretical method. Similarly, the SMA models showed good agreement with ultimate displacements within 5% of the ST values, and yield displacements ranging from 0.97 to 1.09 times those predicted by the theoretical method.

3.3 FRAME-LEVEL MODEL

Static frame modelling

In this study, single-storey BTFs with steel and SMA connections were modelled in OpenSees and subjected to a node-controlled pushover analysis to evaluate their nonlinear response and self-centering behaviour. The analysis was conducted in two stages: a monotonic pushover to determine ultimate displacement, which was validated against the ST method, and a cyclic pushover to assess hysteresis behaviour, energy dissipation, and residual deformation in both connection types.

Timber members were modelled using elastic beam-column elements, while connections were represented by zeroLength elements. Diagonal braces followed calibrated brace-level models. A total of sixteen 2D models -8 with steel and 8 with SMA connections- were developed using SAWS and DTE materials and subjected to horizontal loading at a control node (12), as shown in Figure 7. The timber elements, modelled as 20f-EX glulam with a 127 × 140 mm cross-section, included a 50 kN gravity load to account for P-Delta effects. Frame nodes were free to rotate, and columns were pinned at the base, ensuring timber members remained elastic and all inelastic deformation was concentrated in the brace connections.

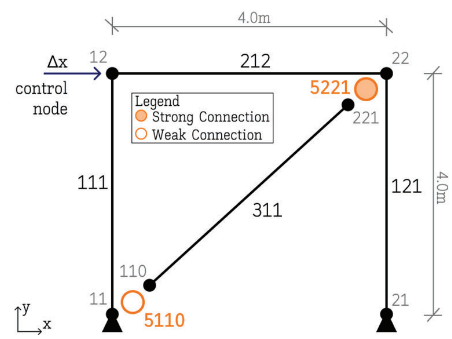

Figure 7: *Pushover analysis - single-storey BTF model*

Dynamic frame modelling

Numerical models were developed in OpenSees to assess the seismic performance of single-storey BTFs with steel and SMA dowel-type connections using nonlinear time history analysis (NTHA). The single-storey frame, previously used for pushover analysis (Figure 7), was extended to dynamic loading to study self-centering behaviour for building induced by seismic events. The frame served to validate the transition from static to dynamic analysis.

Similar to the pushover frame models, the connection springs used the average parameters from the calibrated SAWS and DTE models previously developed. Yield strengths were set at 15.5 kN for steel and 24.1 kN for SMA. All frames were assumed to be located in Ottawa, with loads based on the National Building Code (NBC) of Canada [23]. Gravity loads followed a critical

https://doi.org/10.52202/080513-0183

combination: 100% dead and 25% snow, resulting in 63 kN load equally distributed at the top nodes. Earthquake loads were determined using the equivalent static force procedure assuming Site Class C, with force modification factors based on Chen and Popovski (2020) for a limited ductility BTF.

4 – RESULTS AND DISCUSSION

4.1 PUSHOVER ANALYSIS

To perform the pushover analysis, a gravity analysis was first conducted to establish the initial loading conditions. Gravity loads were applied using a static load pattern and held constant using a load control command to isolate the frame's lateral response. This ensured gravity effects remained fixed during lateral displacement increments. Following this, lateral loads were applied using displacement control through incremental target displacements. This allowed internal forces and deformations to be computed at each step until brace connection failure caused frame instability. The response was captured by plotting base shear versus displacement at the top node, providing insight into nonlinear performance and capacity.

Monotonic Pushover

Frames were loaded laterally until failure. Top displacement and base shear were used to define force-displacement curves for steel and SMA connections using DTE and SAWS material models. Ultimate displacement ($D_{bf,u}$) was taken from OpenSees response curves and compared with theoretical values from spring theory (ST), calculated using the horizontal component of brace displacement ($D_{ba,u}$) and the brace angle. Table 3 shows these comparisons. Results show strong agreement between ST and OpenSees, with differences below 5% for both materials. For the steel connection results, the DTE models matched numerical results slightly closer than the SAWS ones. Both models slightly underestimated displacement compared to ductility-based methods.

Table 3: *Spring Theory and OpenSees Frame Model Results*

Model	ST	OS - DTE		OS - SAWS	
	$D_{bf,u}$	$D_{bf,u}$		$D_{bf,u}$	
4SC1	18.38	17.82	-3.0%	17.81	-3.1%
4SC2	16.86	16.92	0.4%	16.91	0.3%
4SC3	17.05	17.01	-0.2%	16.87	-1.0%
$4SC_{avg}$	17.49	17.27	-1.2%	17.26	-1.3%
4NC1	18.72	18.42	-1.6%	18.27	-2.4%
4NC2	19.50	18.67	-4.2%	18.62	-4.5%
4NC3	21.49	20.47	-4.7%	20.51	-4.5%
$4NC_{avg}$	19.77	19.12	-3.3%	19.11	-3.3%

Cyclic Pushover

To evaluate the cyclic response and self-centering ability of SMA dowels, frame models using average SAWS and DTE parameters were subjected to displacement-controlled loading, following the modified ASTM E2126 Test Method B [20] in the reference experiment from Cléroux et al [18]. Hysteresis curves for the frame models are shown in Figure 8 and closely resemble the weak connection-level responses (Figure 5), confirming that plastic behaviour is governed by the brace connections. Both steel and SMA models showed stable hysteresis under cyclic loading, consistent with previous connection-level results.

The curves revealed post-yield hardening which was more pronounced in the SMA models. While the envelope curves for both material types were similar, SMA-connected frames reached a higher average ultimate displacement of 19.1 mm, compared to 17.3 mm for steel. Both materials exhibited pinched responses, but unloading behaviour differed: steel connections showed permanent deformation, while the loading and unloading branches in the SMA connections passed through the origin demonstrating superelastic behaviour. This aligns with findings from Cléroux et al [18], reinforcing SMA's effectiveness in reducing residual displacement.

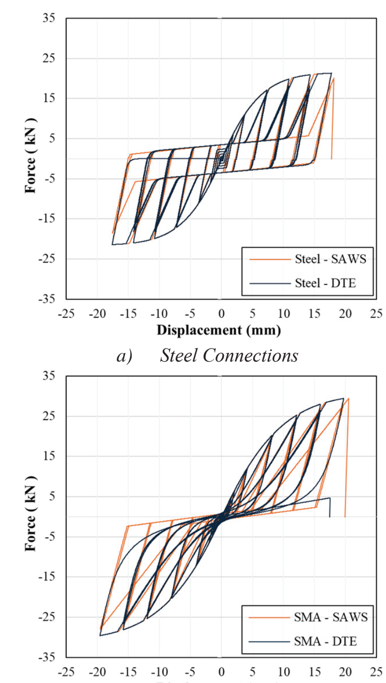

a) Steel Connections

b) SMA Connections

Figure 8: *Single-storey frame – Pushover hysteresis curves*

https://doi.org/10.52202/080513-0183

4.2 TIME HISTORY ANALYSIS

To assess structural dynamic response, a numerical procedure was developed using nonlinear time history analysis (NTHA) in OpenSees. The analysis began with a gravity load step to establish initial conditions, followed by a modal analysis to determine dynamic properties. Eigenvalue analysis was performed using OpenSees functions, assembling stiffness and mass matrices from the model. A damping ratio of 2% critical damping was applied. Modal results provided natural frequencies, mode shapes, and vibration periods. The fundamental natural period was found to be 0.25 seconds. The time history analysis used Newmark's method to compute structural response over time.

In addition, the analysis requires that a deformation capacity be specified to define a limit that, upon exceedance, will stop the NTHA and mark the analysis as a collapse case. For this purpose, a 0.5% peak inter-storey drift (20 mm) was selected—slightly above the maximum brace displacement observed in the pushover analysis. This threshold is applied to the top node's deformation to flag collapse and terminate the simulation. It ensures that the analysis does not continue attempting to converge a model that has effectively collapsed or would be classified as such during post-processing.

Table 4: *Earthquake Record Information and Scaling Factors (SF)*

No.	Event Name	M	R	SF
Eq1	Coyote Lake	5.74	20.67	2.33
Eq2	Livermore-02	5.42	14.12	0.93
Eq3	Mammoth Lakes-02	5.69	16.88	1.60
Eq4	Mammoth Lakes-04	5.70	14.38	1.30
Eq5	Double Springs	5.90	12.84	1.46
Eq6	Ancona-09, Italy	4.70	10.10	1.09
Eq7	Sicilia-Orientale, Italy	5.60	26.93	3.23
Eq8	14151344	5.20	14.19	0.97
Eq9	21465580	4.77	10.07	2.25
Eq10	51182810	4.60	13.42	0.84
Eq11	Morgan Hill	6.19	23.24	1.26
Eq12	Chi-Chi, Taiwan-04	6.20	25.06	1.21
Eq13	Basso Tirreno, Italy	6.00	19.59	0.67
Eq14	Big Bear-01	6.46	26.47	0.89
Eq15	Joshua Tree, CA	6.10	21.97	0.58

Ground motion records were selected to reflect site conditions in Ottawa (Site Class C, V_{S30}: 360 - 760 m/s), located in the Western Quebec Seismic Zone which is characterized by low-to-moderate seismicity and predominantly strike-slip events [24]. Significant earthquakes exceeding magnitude (M) 4.5 have occurred in the region in the past, with no recorded events above M6.5 [25]. Atkinson [26] reported M6 events typically occur 10–30 km from the site with short-period effects (<1.0 sec). Table 4 presents the selected ground motions based on two earthquake scenarios: (1) M4.5-M5.9, and (2) M6-M6.9 at 10-30 km rupture distances (R). Fifteen horizontal acceleration records (Eq1-Eq15) were used, with Eq1-Eq10 corresponding to scenario one and Eq11-Eq15 corresponding to scenario two. Due to limited data in Eastern North America, motions were sourced from Western North America via the PEER database [27]. The ground motions selected were scaled to match the target design spectrum at the fundamental period.

Single Storey Frames

Figure 9 presents the drift response from the time history analysis of a one-storey frame under selected ground motions, including average maximum and residual drift percentages. Results show that although SMA connections produce higher peak displacements due to slightly lower initial stiffness compared to steel, they significantly reduce permanent deformation. Frames with SMA connections reached an average peak drift of 0.15%, compared to 0.095% for steel. The increased drift is attributed to the lower stiffness of SMA connections, allowing more deformation under similar loading. Despite this, SMA frames exhibited superior self-centering behaviour. Residual drift for SMA frames averaged just 0.0014%, significantly lower than the 0.017% observed in steel frames, meaning the residual drift of the steel frames was on average over 12 times larger than that of the SMA frames. These results highlight the effectiveness of SMA connections in reducing residual deformations and post-earthquake damage, enhancing the seismic resilience of single-storey braced frames.

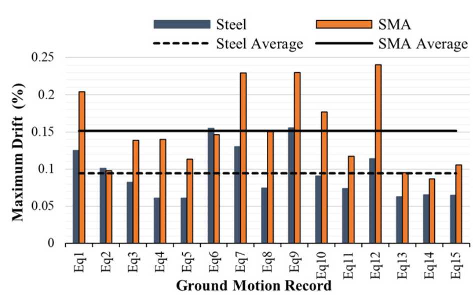

a) *Peak inter-storey drift*

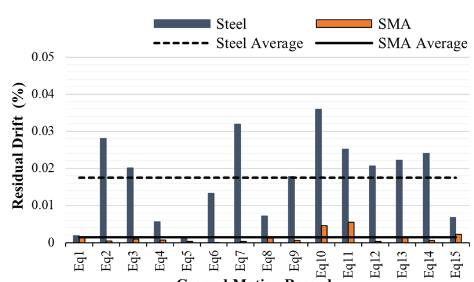

b) *Residual inter-storey drift*

Figure 9: *Single-storey frame – inter storey drifts*

https://doi.org/10.52202/080513-0183

5 – CONCLUSIONS

This study presented an analytical assessment of the seismic performance of BTFs using SMA dowel-type fasteners, as an alternative to traditional steel fasteners. Building upon prior experimental work, the connection-level behaviour of SMA and steel fasteners were modelled in OpenSees and validated using nonlinear numerical simulations based on experimental results. These models were then developed into brace- and frame-level models to evaluate the seismic performance under static and dynamic loading. The study aimed to assess the self-centering ability, energy dissipation, and post-earthquake reparability of SMA-based connections in timber structures. The main findings from the research are summarized as follows:

- Connection-level models for both SMA and steel fasteners were successfully calibrated using OpenSees with SAWS and DTE hysteresis models. The numerical models captured key characteristics of the experimental response, including strength degradation, residual deformation in steel, and the unique loading-unloading behaviour of SMA connections.
- Brace-level modes implemented the weak/strong connection concept and confirmed that nonlinear behaviour is governed by the weaker connection. Numerical results showed strong agreement with analytical spring theory predictions, with discrepancies in yield and ultimate displacements generally below 5% for both material types.
- Frame-level pushover analyses showed that SMA-fasteners models fail at higher ultimate displacements and have a higher post-yielding hardening. Although SMA frames have a reduced stiffness, they achieve comparable strength to steel frames with minimal residual deformation under cyclic loading.
- Nonlinear time history analyses using ground motions representative of seismic hazard levels in Ottawa showed that SMA connections effectively reduced residual inter-storey drift by over 90% compared to steel while allowing slightly higher peak displacements due to their lower initial stiffness. This confirms the self-centering potential of SMA and advantage in post-earthquake reparability in mass timber braced systems.

In summary, SMA dowel-type fasteners demonstrate a strong potential for improving the seismic resilience of braced timber frames by providing significant self-centering behaviour and reducing residual deformations. However, further brace- and frame-level experimental validation is essential to confirm these numerical results. Additional studies on self-centering performance are also needed in representative connections of building brace systems. These investigations should consider the influence of parameters such as fastener slenderness, connection geometry, and dowel size, which may significantly impact the global seismic response of larger structural systems.

6 – REFERENCES

[1] Z. Chen and M. Popovski, “Expanding wood use towards 2025: seismic performance of braced mass timber frames, Year 2,” FPInnovations, 2020.

[2] Z. Chen and M. Popovski, “Seismic Response of Braced Heavy Timber Frames with Riveted Connections (Y1),” *J. Perform. Constr. Facil.*, vol. 35, no. 5, p. 04021051, Oct. 2021, doi: 10.1061/(ASCE)CF.1943-5509.0001618.

[3] CSA, *Canadian Standards Association, CSA 086: Engineering Design in Wood*, Canada., 2019.

[4] M. Popovski, “Structural Systems with Riveted Connections for Non-Residential Buildings,” *Resid. Build.*, 2004.

[5] M. Popovski, H. G. L. Prion, and E. Karacabeyli, “Seismic performance of connections in heavy timber construction,” *Can. J. Civ. Eng.*, vol. 29, no. 3, pp. 389–399, Jun. 2002, doi: 10.1139/l02-020.

[6] M. Popovski, H. G. L. Prion, and E. Karacabeyli, “Shake table tests on single-storey braced timber frames,” *Canadian Journal of Civil Engineering*, vol. 30, no. 6, pp. 1089–1100, 2003, doi: 10.1139/L03-060.

[7] M. Popovski, “Seismic performance of braced timber frames,” University of British Columbia, 2000. [Online]. Available: https://dx.doi.org/10.14288/1.0064074

[8] Z. Chen and M. Popovski, “Connection and System Ductility Relationship for Braced Timber Frames (Y2),” *J. Struct. Eng.*, vol. 146, no. 12, p. 04020257, Dec. 2020, doi: 10.1061/(ASCE)ST.1943-541X.0002839.

[9] Z. Baird, J. Woods, C. Viau, and G. Doudak, “SEISMIC PERFORMANCE OF BOLTED GLULAM TIMBER BRACE CONNECTIONS WITH INTERNAL STEEL PLATES,” in *World Conference on Timber Engineering (WCTE 2023)*, Oslo, Norway: World Conference on Timber Engineering (WCTE 2023), 2023, pp. 1176–1182. doi: 10.52202/069179-0161.

[10] C. Murphy, C. P. Pantelides, H.-E. Blomgren, and D. Rammer, “Development of Timber Buckling Restrained Brace for Mass Timber-Braced

https://doi.org/10.52202/080513-0183

Frames," *J. Struct. Eng.*, vol. 147, no. 5, p. 04021050, May 2021, doi: 10.1061/(ASCE)ST.1943-541X.0002996.

[11] T. Takeuchi, Y. Terazawa, S. Komuro, T. Kurata, and B. Sitler, "Performance and failure modes of mass timber buckling-restrained braces under cyclic loading," *Eng. Struct.*, vol. 266, p. 114462, Sep. 2022, doi: 10.1016/j.engstruct.2022.114462.

[12] E. Williamson, C. P. Pantelides, H.-E. Blomgren, and D. Rammer, "Seismic Performance of Timber Frames with Timber Buckling-Restrained Braces," *J. Struct. Eng.*, vol. 150, no. 6, p. 04024048, Jun. 2024, doi: 10.1061/JSENDH.STENG-12877.

[13] B. Folz and A. Filiatrault, "Seismic Analysis of Woodframe Structures. I: Model Formulation," *J. Struct. Eng.*, vol. 130, no. 9, pp. 1353–1360, Sep. 2004, doi: 10.1061/(ASCE)0733-9445(2004)130:9(1353).

[14] H. Dong, M. He, X. Wang, C. Christopoulos, Z. Li, and Z. Shu, "Development of a uniaxial hysteretic model for dowel-type timber joints in OpenSees," *Constr. Build. Mater.*, vol. 288, p. 123112, Jun. 2021, doi: 10.1016/j.conbuildmat.2021.123112.

[15] H. Huang, W.-S. Chang, and K. Chen, "Study of SMA-dowelled timber connection reinforced by densified veneer wood under cyclic loading," *MATEC Web Conf.*, vol. 275, p. 01015, 2019, doi: 10.1051/matecconf/201927501015.

[16] H. Huang and W.-S. Chang, "Seismic resilience timber connection-adoption of shape memory alloy tubes as dowels," *Struct. Control Health Monit.*, vol. 24, no. 10, p. e1980, Oct. 2017, doi: 10.1002/stc.1980.

[17] R. Schwarze, M. Braun, W. Seim, P. Krooß, M. Vollmer, and T. Niendorf, "Application and potential of shape memory alloys for dowel-type connections in timber structures," *Wood Mater. Sci. Eng.*, vol. 17, no. 6, pp. 636–647, Nov. 2022, doi: 10.1080/17480272.2021.1920625.

[18] M. Cléroux, E. Kim, and D. Lacroix, "Cyclic Behavior and Damage Assessment of Superelastic SMA Dowel Connections for Braced Timber Frame Applications," *J. Perform. Constr. Facil.*, vol. 38, no. 5, p. 04024027, Oct. 2024, doi: 10.1061/JPCFEV.CFENG-4686.

[19] S. Mazzoni, F. McKenna, M. H. Scott, and G. L. Fenves, *OpenSees Version 1: Open system for earthquake engineering simulation user command-language manual*, 3, 2006.

[20] ASTM, *Standard Test Methods for Cyclic (Reversed) Load Test for Shear Resistance of Vertical Elements of the Lateral Force Resisting Systems for Buildings*, 2019.

[21] K. W. Johansen, "Theory of Timber Connections," *Int. Assoc. Bridge Struct. Eng. IABSE Publ.*, vol. 9, pp. 249–262, 1949, doi: 10.5169/SEALS-9703.

[22] Z. Baird, J. E. Woods, C. Viau, and G. Doudak, "Cyclic Behavior of Bolted Glued-Laminated Timber Brace Connections with Slotted-In Steel Plates," *J. Struct. Eng.*, vol. 150, no. 7, p. 04024068, Jul. 2024, doi: 10.1061/JSENDH.STENG-13012.

[23] NBC, *National Building Code of Canada 2020 (NBCC 2020)*, 2020.

[24] R. E. Rimando and K. Benn, "Evolution of faulting and paleo-stress field within the Ottawa graben, Canada," *J. Geodyn.*, vol. 39, no. 4, pp. 337–360, May 2005, doi: 10.1016/j.jog.2005.01.003.

[25] S. Ma and D. W. Eaton, "Western Quebec seismic zone (Canada): Clustered, midcrustal seismicity along a Mesozoic hot spot track," *J. Geophys. Res. Solid Earth*, vol. 112, no. B6, p. 2006JB004827, Jun. 2007, doi: 10.1029/2006JB004827.

[26] G. M. Atkinson, "Earthquake time histories compatible with the 2005 *National building code of Canada* uniform hazard spectrum," *Can. J. Civ. Eng.*, vol. 36, no. 6, pp. 991–1000, Jun. 2009, doi: 10.1139/L09-044.

[27] T. Ancheta *et al.*, "NGA-West2 Database," *Earthq. Spectra*, vol. 30, no. 3, pp. 989–1005, Aug. 2014, doi: https://doi.org/10.1193/070913eqs197m.

 https://doi.org/10.52202/080513-0183